NUMERICAL STUDY OF THERMAL RADIATIONS AND THERMAL STRATIFICATION MECHANISMS IN MAGNETOHYDRODYNAMIC CASSON FLUID-FLOW

by

Khalil Ur REHMAN [a,b*], ***Noor Ul SABA*** [a], ***Iffat ZEHRA*** [b], ***Muhammad Yousaf MALIK*** [a,c], ***and Sardar Muhammad BILAL*** [b]

[a] Department of Mathematics, Quaid-i-Azam University, Islamabad, Pakistan
[b] Department of Mathematics, Air University, Islamabad, Pakistan
[c] Department of Mathematics, Faculty of Science, King Abdulaziz University, Jeddah, Saudi Arabia

Original scientific paper
https://doi.org/10.2298/TSCI180424192R

The features of Casson liquid when flow field is thermally stratified are offered in this article. The flow is taken through an inclined cylinder with both MHD fluid and thermal radiations assumptions. A mathematical model is constructed in terms of differential equations via fundamental laws. Since the resultant system is non-linear so a self-coded computational algorithm is implemented to report numerical solution. The obtain observations in this regard are presented by way of both tabular and graphical trends. It is noticed that the Casson fluid temperature is decreasing function of thermal stratification parameter while opposite trend is observed via thermal radiation parameter. Moreover, the cylindrical geometry admits enlarged variations towards involved physical parameters as compared to flat surface.

Key words: *MHD fluid, thermal radiations, temperature stratification, heat generation, heat absorption, Casson fluid, inclined surface*

Introduction

An analysis on non-Newtonian fluids has always become a topic of great interest among the researchers because of its wide range of uses in engineering and industry. The fluid model used in this analysis is Casson fluid and it has huge applications in the field of food processing, metallurgy and bioengineering operations to mention just a few. The Casson fluid model has got popularity because of the success of the experimental and theoretical investigations, see [1, 2]**.** In 1959, the Casson fluid was first identified by Casson. The Casson fluid is well-defined as a shear thinning fluid having an infinite viscosity at zero shear rate [3]. If a shear stress applied to the fluid is less than the yield stress, Casson turns into a solid but it starts moving for the case greater shear stress as compared to yield stress. By keeping in view all these aspects, the Casson fluid-flow via various geometries is discussed by the researchers like Kameswaran *et al.* [4] addressed the dual solution of Casson fluid-flow yielded by flat surface. The time dependent flow of Casson fluid was reported by Khalid *et al.* [5]. Animasaun [6] offered non-Darcy flow of Casson liquid manifested with n^{th} order chemical reaction. By considering the Casson fluid model, the effects of ferrous nanoparticles was studied by Raju and Sandeep [7].

* Corresponding author, e-mail: krehman@math.qau.edu.pk

Recently, Nawaz *et al.* [8] worked on variable thermal conductivity aspects subject to Casson fluid model. The recent developments regarding the Casson fluid-flow can be assessed in [9, 10].

The fluid having interaction with magnetic field is termed as MHD flow. Such combination claims significant number of applications like wound healing, magnetic reason imaging (MRI) and canter action causing hypothermia, *etc.* Even the metals fusion and cooling process involved the use of externally applied magnetic field. Owning the importance of MHD flows various efforts are shared by investigators like Chakrabarti and Gupta [11] studied MHD flow of Newtonian fluid model. The non-Newtonian fluid-flow along with MHD effect was discussed by Akbar *et al.* [12]. Since than one can assessed the literature regarding MHD analysis in [13-25].

The effects of thermal radiation claims a vital role in the industrial and engineering processes. These processes include performance at an extreme temperature under different non-isothermal conditions and instance where convective heat transfer coefficient are lower. Thermal radiations are type of electromagnetic radiations that are emitted in the form of energy. These radiations travel with a speed equal to the speed of light and do not require any type of medium for their propagation. The effect of thermal radiation parameter on MHD flow towards heated surface was given by Rahman and Salahuddin [26]. Many researchers [27-29] acknowledged the importance of contribution of thermal radiations, mixed convection and suggested definitive significances.

From the aforementioned limited literature study, it is determined that few attempts are available to encountered the Casson fluid-flow towards a cylindrical surface. To be more precise, the combined aspects of thermal radiations and stratification phenomena in a magnetized flow field is not discussed yet. An attempt is attractive in this sense it contains simultaneous analysis for both an inclined cylinder and flat geometry. The flow is accomplished by considering no slip conditions. The physical effects involved in this paper includes stagnation point, mixed convection, magnetic field, and heat generation/absorption. A numerical solution is presented by means of shooting method and ultimate findings are reported with the aid of both graphs and tables.

Mathematical formulation

In the present work, MHD incompressible boundary-layer flow of a Casson fluid under the region of stagnation point is considered. The no slip condition is applied on the fluid-flow that is the stretching velocity of geometry resemble with the velocity of the fluid particles. In addition, heat generation, thermal radiation and stratification phenomenon, mixed convection effects are also taken into account. It is important to note that the destruction of fluctuation velocity gradients by the action of viscous stresses in a laminar boundary-layer flow of Casson fluid is assumed to be small, so that the viscous dissipation is ignored [29]. Near the cylindrical surface, the strength of temperature is higher than that of ambient fluid. For the geometrical representation, we have taken the cylinder axial line along $\hat{X}$-axis and the radial direction is adjusted normal to the fluid-flow, $\hat{R}$-axis. The most acknowledged differential equations in the field of fluid science are the energy and the momentum equations. They are enough to demonstrate the flow field properties. So that the complete model of these equations [9, 10] based on the boundary-layer approximations are given:

$$\frac{\partial\left(\hat{R}\hat{U}\right)}{\partial\hat{X}}+\frac{\partial\left(\hat{R}\hat{V}\right)}{\partial\hat{R}}=0 \tag{1}$$

$$\hat{U}\frac{\partial \hat{U}}{\partial \hat{X}}+\hat{V}\frac{\partial \hat{U}}{\partial \hat{R}}=\nu\left(1+\frac{1}{\beta}\right)\left(\frac{\partial^2 \hat{U}}{\partial \hat{R}^2}+\frac{1}{R}\frac{\partial \hat{U}}{\partial \hat{R}}\right)+\hat{U}_e\frac{\partial \hat{U}_e}{\partial \hat{X}}-\frac{\sigma B_0{}^2}{\rho}\left(\hat{U}-\hat{U}_e\right)+g_0\beta_T\left(\hat{T}-\hat{T}_\infty\right)\cos\alpha \tag{2}$$

$$\hat{U}\frac{\partial \hat{T}}{\partial \hat{X}}+\hat{V}\frac{\partial \hat{T}}{\partial \hat{R}}=\alpha^\bullet\left(\frac{1}{\hat{R}}\frac{\partial \hat{T}}{\partial \hat{R}}+\frac{\partial^2 \hat{T}}{\partial \hat{R}^2}\right)-\frac{1}{\rho c_p \hat{R}}\frac{\partial}{\partial \hat{R}}(\hat{R}q_{\hat{R}})+\frac{Q_0}{c_p\rho}(\hat{T}-\hat{T}_\infty) \tag{3}$$

where

$$\hat{q}_{\hat{R}}=-\left(\frac{4}{3}\right)\frac{\alpha^\bullet}{k^\bullet}\frac{\partial \hat{T}^4}{\partial \hat{R}}$$

represents the Rosseland radiative heat flux. Accordingly, we can reorganize eq. (3):

$$\hat{U}\frac{\partial \hat{T}}{\partial \hat{X}}+\hat{V}\frac{\partial \hat{T}}{\partial \hat{R}}=\alpha^\bullet\left(\frac{1}{\hat{R}}\frac{\partial \hat{T}}{\partial \hat{R}}+\frac{\partial^2 \hat{T}}{\partial \hat{R}^2}\right)+\frac{1}{\rho c_p \hat{R}}\left(\frac{4}{3}\right)\frac{\sigma^\bullet}{k^\bullet}\frac{\partial}{\partial \hat{R}}\left(\hat{R}\frac{\partial \hat{T}^4}{\partial \hat{R}}\right)+\frac{Q_0}{\rho c_p}(\hat{T}-\hat{T}_\infty) \tag{4}$$

with

$$\begin{gathered}\hat{U}=\hat{U}(\hat{X})=\frac{U_0}{L}\hat{X},\quad V=0,\quad \hat{T}(\hat{X},\hat{R})=\hat{T}_w(\hat{X})=\hat{T}_0+\frac{c\hat{X}}{L},\quad \text{at}\quad \hat{R}=b\\ \hat{U}\to\hat{U}_e=\frac{U_0^\bullet}{L}\hat{X},\quad \hat{T}(\hat{X},\hat{R})\to\hat{T}_\infty(\hat{X})=\hat{T}_0+\frac{d}{L}\hat{X},\quad \text{as}\quad \hat{R}\to\infty\end{gathered} \tag{5}$$

where $\hat{V}$, $(\hat{X}, \hat{R})$ and $\hat{U}$ $(\hat{X}, \hat{R})$ are velocity components in $\hat{R}$- and $\hat{X}$-direction, respectively. Moreover, c, d, L, $\hat{T}_w$, $(\hat{X})$, Q_0, $\hat{T}_\infty$, $\hat{T}$, c_p, α, $\alpha^\bullet$, β_T, B_0, σ, g_0, $\hat{U}_e$, β, ρ, and ν, represents dimensionless constants, reference length, arbitrary surface temperature, heat generation coefficient, ambient temperature, fluid temperature, specific heat capacity at constant pressure, thermal diffusivity, an inclination, thermal expansion coefficient, acceleration due to gravity, uniform magnetic field, electrical conductivity, free stream velocity, Casson fluid parameter, fluid density, and kinematics viscosity, respectively. For the solution of eqs. (2)-(4) along with the boundary conditions given by eq. (5), we have assumed the transformation [9, 10, 30, 31]**:**

$$\begin{gathered}\hat{U}=\frac{\hat{U}_0\hat{X}}{L}F'(\eta),\quad \hat{V}=-\frac{b}{\hat{R}}\sqrt{\frac{U_0\nu}{L}}F(\eta),\quad \eta=\frac{\hat{R}^2-b^2}{2b}\sqrt{\frac{U_0}{\nu L}},\\ \psi=\sqrt{\frac{U_0\nu\hat{X}^2}{L}}\,bF(\eta),\quad T(\eta)=\frac{\hat{T}-\hat{T}_\infty}{\hat{T}_w-\hat{T}_0}\end{gathered} \tag{6}$$

where ψ, $\hat{T}_0$, $F'(\eta)$, $F(\eta)$, b, and U_0 represents stream function, reference temperature, fluid velocity, dimensionless variable, radius of cylinder, and reference velocity, respectively. The eq. (1) identically fulfills and acknowledged by the stream function:

$$\hat{U}=\frac{1}{\hat{R}}\left(\frac{\partial\psi}{\partial \hat{R}}\right),\qquad \hat{V}=-\frac{1}{\hat{R}}\left(\frac{\partial\psi}{\partial \hat{X}}\right) \tag{7}$$

use of eq. (6) into eqs. (2)-(5) results:

$$\begin{gathered}\left(1+\frac{1}{\beta}\right)\left[(1+2K\eta)\frac{\mathrm{d}^3F(\eta)}{\mathrm{d}\eta^3}+2K\frac{\mathrm{d}^2F(\eta)}{\mathrm{d}\eta^2}\right]+F(\eta)\frac{\mathrm{d}^2F(\eta)}{\mathrm{d}\eta^2}-\\ -\left(\frac{\mathrm{d}F(\eta)}{\mathrm{d}\eta}\right)^2-\gamma^2\left(\frac{\mathrm{d}F(\eta)}{\mathrm{d}\eta}-A\right)+A^2+\lambda T(\eta)\cos\alpha=0\end{gathered} \tag{8}$$

$$3\left(1+2K\eta\right)\left(3+4R_d\right)\frac{\mathrm{d}^2T(\eta)}{\mathrm{d}\eta^2}+6K\left(3+4R_d\right)\frac{\mathrm{d}T(\eta)}{\mathrm{d}\eta}+$$
$$+3\Pr\left(F(\eta)\frac{\mathrm{d}T(\eta)}{d\eta}-\frac{\mathrm{d}F(\eta)}{\mathrm{d}\eta}\delta_1+QT(\eta)\right) \tag{9}$$

with

$$\frac{\mathrm{d}F(\eta)}{\mathrm{d}\eta}=1,\quad F(\eta)=0,\quad T(\eta)=1-\delta_1,\quad \text{at}\quad \eta=0,$$
$$\frac{\mathrm{d}F(\eta)}{\mathrm{d}\eta}\to A,\qquad T(\eta)\to 0,\quad \text{when}\quad \eta\to\infty \tag{10}$$

where Q, δ_1, Pr, R_d, λ_m, A, γ, and K heat generation/absorption, thermal stratification, Prandtl number, thermal radiation, mixed convection, velocities ratio, magnetic field and curvature parameters, respectively and they are described:

$$K=\frac{1}{\widehat{R}}\sqrt{\frac{\nu L}{U_0}},\quad \gamma=\sqrt{\frac{\sigma B_0{}^2L}{\rho U_0}},\quad \lambda=\frac{\mathrm{Gr}}{\mathrm{Re}_{\widehat{X}}^2},\quad R_d=\frac{4\sigma^\bullet T_\infty{}^3}{k^\bullet k},\quad A=\frac{U_0^\bullet}{U_0}$$
$$\Pr=\frac{\nu}{\alpha^\bullet},\quad \delta_1=\frac{d}{c},\quad \mathrm{Gr}=\frac{\mathrm{g}_0\beta_T\left(\widehat{T}_w-\widehat{T}_0\right)\widehat{X}^3}{\nu^2},\quad Q=\frac{LQ_0}{U_0\rho c_p} \tag{11}$$

At the cylindrical surface, the skin friction coefficient (SFC) is written:

$$C_F=\frac{\tau_w}{\rho\frac{U^2}{2}},\qquad \tau_w=\mu\left(1+\frac{1}{\beta}\right)\left(\frac{\partial\widehat{U}}{\partial\widehat{R}}\right)_{\widehat{R}=b} \tag{12}$$

where μ and τ_w expresses the fluid viscosity and the shear stress correspondingly. The non-dimensional expression we have:

$$\frac{1}{2}C_F\sqrt{\mathrm{Re}_{\widehat{X}}}=\left(1+\frac{1}{\beta}\right)\frac{d^2F(\eta)}{d\eta^2}\quad \text{at}\quad \eta=0 \tag{13}$$

where

$$\mathrm{Re}_{\widehat{X}}=\frac{U_0\widehat{X}^2}{\nu L}$$

describes the local Reynolds number. The expression for the local Nusselt number (LNN) is given:

$$\mathrm{Nu}_{\widehat{X}}=\frac{\widehat{X}q_w}{k(\widehat{T}_w-\widehat{T}_0)},\quad q_w=-k\left(\frac{\partial\widehat{T}}{\partial\widehat{R}}\right)_{\widehat{R}=b}+\left(q_{\widehat{R}}\right)_{\widehat{R}=b} \tag{14}$$

the dimensionless form is pre-arranged:

$$\frac{\mathrm{Nu}_{\widehat{X}}}{\sqrt{\mathrm{Re}_{\widehat{X}}}}=-\left(1+\frac{4}{3}R_d\right)\frac{\mathrm{d}T(\eta)}{\mathrm{d}\eta}\quad \text{at}\quad \eta\to 0 \tag{15}$$

Computational scheme

For the implementation of the computational scheme, firstly we have converted the PDE into system of ODE. To be more specific, eqs. (8) and (9) are coupled non-linear ODE with eq. (10), and are solved by making use of the shooting scheme [30, 31]. For this purpose, we have reduced the given equations into a system of five first order ODE, by captivating:

$$M_1 = F(\eta),\ M_2 = \frac{\mathrm{d}F(\eta)}{\mathrm{d}\eta},\ M_3 = \frac{\mathrm{d}M_2(\eta)}{\mathrm{d}\eta} = \frac{\mathrm{d}^2F(\eta)}{\mathrm{d}\eta^2}$$
$$M_4 = T(\eta),\ M_5 = \frac{\mathrm{d}M_4(\eta)}{\mathrm{d}\eta} = \frac{\mathrm{d}T(\eta)}{\mathrm{d}\eta} \tag{16}$$

by making the use of previous replacements, the identical form of eqs. (8)-(9) depending on the new variables is given:

$$\frac{\mathrm{d}M_1}{\mathrm{d}\eta} = M_2,\quad \frac{\mathrm{d}M_2}{\mathrm{d}\eta} = M_3$$
$$\frac{\mathrm{d}M_3}{\mathrm{d}\eta} = \frac{\gamma^2(M_2 - A) - A^2 - \lambda\cos\alpha M_4 + (M_2)^2 - M_1M_3 - 2KM_3\left(1+\dfrac{1}{\beta}\right)}{\left(1+\dfrac{1}{\beta}\right)(1+2K\eta)} \tag{17}$$
$$\frac{\mathrm{d}M_4}{\mathrm{d}\eta} = M_5,\quad \frac{\mathrm{d}M_5}{\mathrm{d}\eta} = \frac{3\,\mathrm{Pr}(M_2M_4 + \delta_1M_2 - M_1M_5 - QM_4) - 6K(3+4R_d)M_5}{3(1+2K\eta)(3+4R_d)}$$

with

$$M_1(0) = 0,\quad M_2(0) = 1,\quad M_3(0) = \omega_1,\quad M_4(0) = 1-\delta_1,\quad M_5(0) = \omega_2 \tag{18}$$

where ω_1 *and* ω_2 are designated as the initial guessed values. For the integration of eq. (17), it must be mandatory that we have:

$$M_3(\eta) = \frac{\mathrm{d}^2F(\eta)}{\mathrm{d}\eta^2} \quad \text{and} \quad M_5(\eta) = \frac{\mathrm{d}T(\eta)}{\mathrm{d}\eta}, \quad \text{when} \quad \eta \to 0 \tag{19}$$

beside this, we have observed that the two initial conditions explicitly $M_3(\eta)$ and $M_5(\eta)$ when $\eta \to 0$ are not known but we do have:

$$M_2(\eta) = A \quad \text{and} \quad M_4(\eta) = 0 \quad \text{when} \quad \eta \to \infty \tag{20}$$

The integration of eq. (17) are carried in such a way that the eq. (20) satisfies completely.

Results and discussion

Velocity profiles

The computational algorithm is implemented with following values of involved parameters that is $\gamma = 0.1$, $A = 0.1$, $K = 0.1$, $\lambda = 0.1$, $\alpha = 45°$ or $0°$, $\beta = 0.3$, $\mathrm{Pr} = 0.7$, $\delta_1 = 0.1$, $Q = 0.1$, and $R_d = 0.1$. The numerical values of the skin friction coefficient (SFC) are provided with the help of tabs. 1 and 2 for the positive values of different parameters namely, K, γ, A, β, λ, and Q. In detail, it is found the SFC (in absolute sense) is found to be an increasing function of K, γ, and β, while it shows an opposite attitude for A and λ. However, the tab. 2 clearly depicts

Table 1. Variations in SFC via *K*, *γ*, and *A*

K	γ	A	$F''(0)$	$0.5C_F\sqrt{\mathrm{Re}_{\bar{X}}}=\left(1+\dfrac{1}{\beta}\right)F''(0)$
0.1	0.1	0.1	–0.4095	–0.8190
0.2	0.1	0.1	–0.5268	–1.0536
0.3	0.1	0.1	–0.6541	–1.3082
0.1	0.2	0.1	–0.4126	–0.8252
0.1	0.4	0.1	–0.4249	–0.8498
0.1	0.6	0.1	–0.4448	–0.8896
0.1	0.1	0.1	–0.4095	–0.8190
0.1	0.1	0.3	–0.3433	–0.6866
0.1	0.1	0.5	–0.2616	–0.5232

Table 2. Variations in SFC via *β, λ*, and *Q*

β	λ	Q_+	$F''(0)$	$0.5C_F\sqrt{\mathrm{Re}_{\bar{X}}}=\left(1+\dfrac{1}{\beta}\right)F''(0)$
0.4	0.1	0.1	–0.6187	–1.2374
0.6	0.1	0.1	–0.6920	–1.3840
0.8	0.1	0.1	–0.7435	–1.4870
0.1	0.3	0.1	–0.4044	–0.8088
0.1	0.5	0.1	–0.3993	–0.7986
0.1	0.7	0.1	–0.3943	–0.7886
0.1	0.1	0.4	–0.4095	–0.8190
0.1	0.1	0.5	–0.4095	–0.8190
0.1	0.1	0.6	–0.4095	–0.8190

that the SFC is independent of different values of Q_+. In other words, the SFC shows constant values for different positive values of Q_+. Negative sign involved in tabs. 1 and 2 physically represents the amount of drag force offered by cylindrical surface to the Casson fluid particles. Further, the negative sign subject to tabs. 3 and 4 indicated the rate of heat transfer normal to the cylindrical surface. The effects of various physical parameters namely β, K, λ, γ, and A on the Casson fluid velocity (CFV) are represented with the aid of figs. 1-4. To be more specific, in fig. 1, the impact of Casson fluid parameter on the velocity profile is given. It has been observed through the figure that the velocity profile shows a decrease in the behavior for both the surfaces by increasing the value of the β. Figure 2 is plotted to observe the attitude of the K on CFV. It shows that the increasing values of the K represents an increase in the CFV for both surfaces (flat and cylinder). For the radius of curvature, the curvature parameter shows a reverse attitude. An increment in curvature parameters brings decreasing values of radius of cylinder. This reduces the contact surface area of surface with the Casson fluid particles which yields less resistance and as a results CFV increases. Figure 3 represents the impact of the λ on the velocity profile for the Casson fluid for both surfaces. It has been observed that the higher values of the λ brings an increase in the CFV, which is in fact due to the appealing behavior of the thermal

Table 3. Variations in LNN via *K*, *γ*, and *A*

K	γ	A	$T'(0)$	$\frac{\mathrm{Nu}}{\sqrt{\mathrm{Re}_{\bar{X}}}} - \left(1+\frac{4}{3}R_d\right)T'(0)$
0.2	0.1	0.1	–0.4279	0.4850
0.4	0.1	0.1	–0.7066	0.8008
0.6	0.1	0.1	–0.9898	1.1217
0.1	0.1	0.1	–0.3038	0.3443
0.1	0.3	0.1	–0.3035	0.3440
0.1	0.5	0.1	–0.3028	0.3432
0.1	0.1	0.1	–0.3038	0.3443
0.1	0.1	0.2	–0.3067	0.3476
0.1	0.1	0.3	–0.3098	0.3511

Table 4. Variations in LNN via *β*, *λ*, and *Q*

β	λ	Q_+	$T'(0)$	$\frac{\mathrm{Nu}}{\sqrt{\mathrm{Re}_{\bar{X}}}} - \left(1+\frac{4}{3}R_d\right)T'(0)$
0.7	0.1	0.1	–0.2929	0.3319
0.8	0.1	0.1	–0.2923	0.3313
0.9	0.1	0.1	–0.2918	0.3307
0.1	0.3	0.1	–0.3041	0.3446
0.1	0.4	0.1	–0.3043	0.3449
0.1	0.5	0.1	–0.3044	0.3450
0.1	0.1	0.1	–0.3038	0.3443
0.1	0.1	0.4	–0.2900	0.3287
0.1	0.1	0.7	–0.2758	0.3126

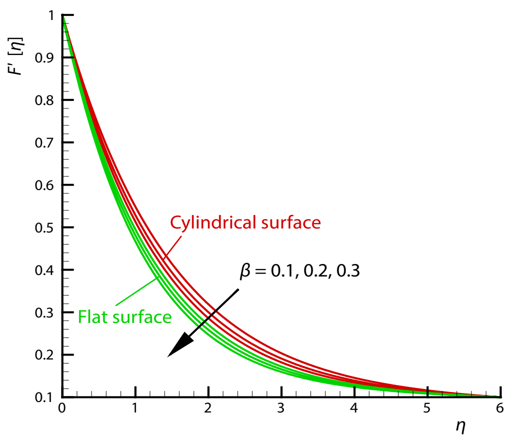

Figure 1. Impact of *β* on CFV

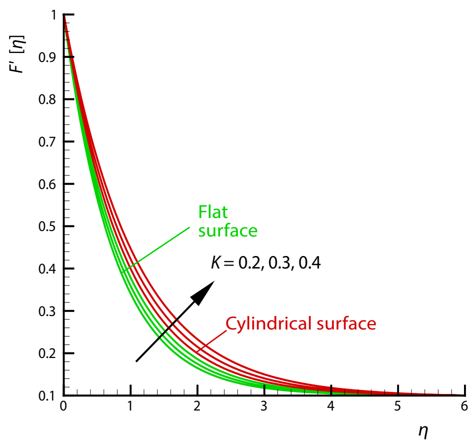

Figure 2. Impact of *K* on CFV

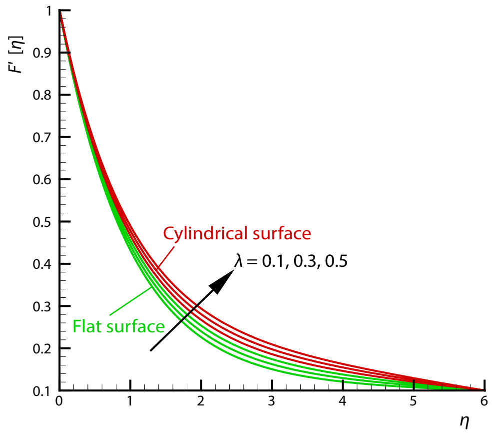

Figure 3. Impact of λ on CFV

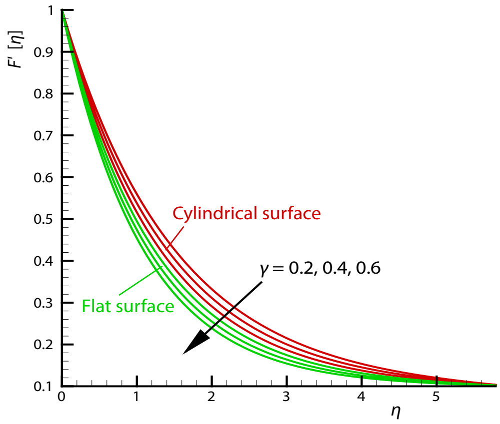

Figure 4. Impact of γ on CFV

buoyancy forces. Figure 4 represents the influence of the magnetic field parameter on the CFV. The increasing values of the magnetic field parameter brings a decrease in the velocity profile for cylindrical and the flat surfaces. In real exercise, by increasing the magnetic field parameter, a resistive force called the Lorentz force subsidize effectively which offers resistance to the fluid particles and as a result of this the horizontal velocity of the fluid decreases. For fig. 5 it is clear that the CFV is increasing function of velocity ratio parameter.

Temperature profiles

Tables 3 and 4 expresses the impact of K, γ, A, β, λ, and Q_+ on the LNN. It is noticed that the LNN shows an inciting attitude towards the higher values of K, A, and λ however it shows a decline behavior towards increasing values of γ, β, and Q_+.

The influences of an involved parameters namely, δ_1, Q_+, Q_-, R_d, K, and Prandtl number on the CFT are represented by means of figs. 6-11. In detail, the behavior of the temperature distribution towards δ_1 is identified in fig. 6. It is noticed that the temperature profile shows decline curves for both the surfaces for increasing values of the δ_1. This actually happens due

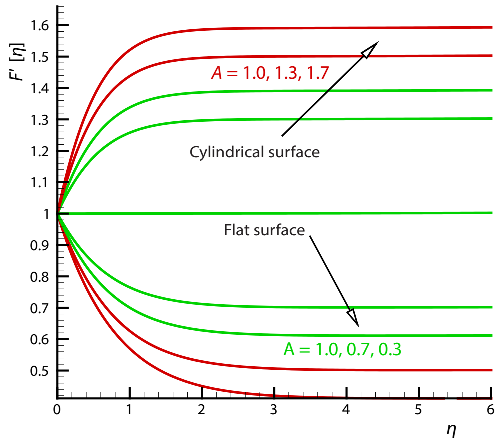

Figure 5. Impact of A on CFV

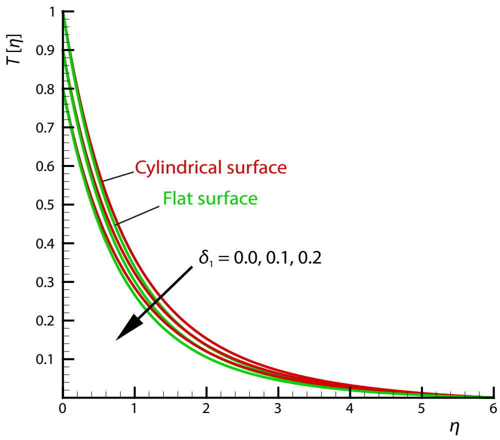

Figure 6. Impact of δ_1 on CFT

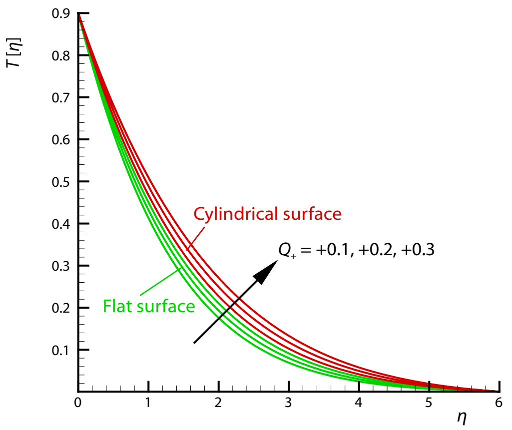

Figure 7. Impact of Q_+ on CFT

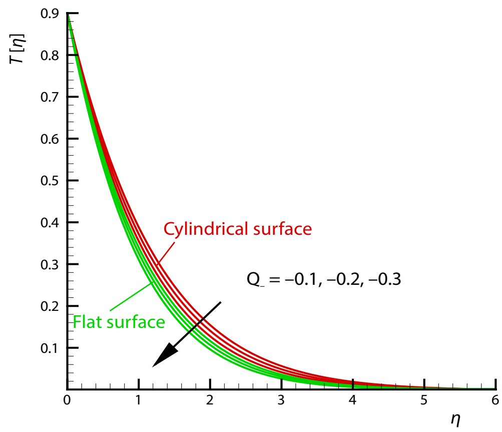

Figure 8. Impact of Q_- on CFT

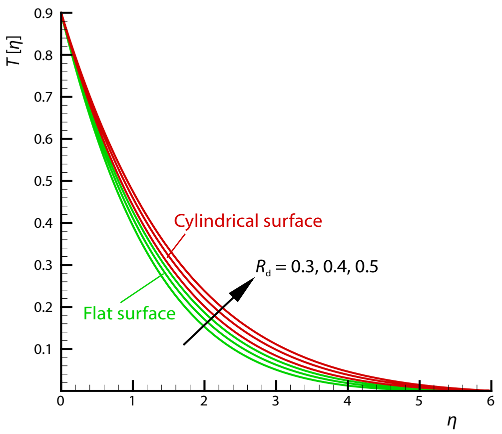

Figure 9. Impact of R_d on CFT

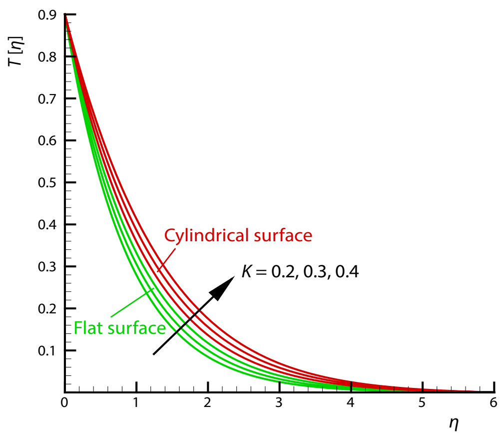

Figure 10. Impact of *K* on CFT

to the drop in temperature difference between ambient fluid and surface of cylinder and hence the temperature profile shows a decreasing values. Figure 7 is plotted to observe the impact of the Q_+ on the CFT. It is noticed that the CFT increases while opposite behavior is observed for the heat absorption parameter depicted in fig. 8. This all happens because heat energy is produced via heat generation process that brings an improvement in temperature while in the case of heat absorption parameter, heat energy is released and as a results decrease in temperature distribution is witnessed for the Casson fluid. Figure 9 portrays the attitude of the temperature profile towards R_d. It is observed that for both surfaces the temperature profile shows an incit-

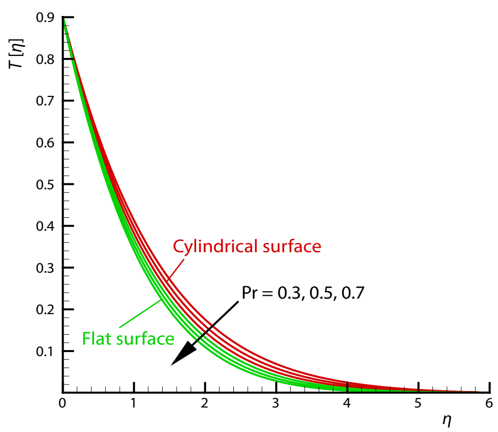

Figure 11. Impact of Prandtl number on CFT

ing attitude towards the R_d. The large values of thermal radiation parameter corresponds significant amount of transfer of heat so that the temperature of flow regime enhanced. Figure 10 depicts the temperature variationwards the K. It is clearly observed that by increasing the values of the curvature parameter, the temperature profile also shows an inciting behavior for cylindrical as well as the flat surface. The positive values of K reflects decrease in radius of cylinder so that lesser resistance is faced by Casson fluid particles and average kinetic energy enhances so that the fluid temperature shows inciting traits because Kelvin temperature is defined as an average kinetic energy. The influence of the temperature profile against the Prandtl number is demonstrate in fig. 11. It is clear from the figure that an increase in the Prandtl number causes a strong reduction in the temperature distribution, which makes the thermal boundary-layer thin. As Prandtl number admits inverse relation with the thermal conductivity, so increasing values of Prandtl number corresponds less diffusion of energy because of which a decrease in the CFT is noticed. The obtain results are validated via comparison with existing literature. We found an excellent match. Table 5 is constructed in this direction.

Table 5. Comparative values of $NU_{\bar{x}}/(\mathrm{Re}_{\bar{x}})^{1/2} = -T'(0)$ towards Prandtl number

Pr	[32] $E = K = 0$	[33] $St = S = M = 0$	Present outcomes $\beta \to \infty$, $K = \delta_1 = \gamma = Q = 0$, $\alpha = 0^0$, $A = 0$, $R_d = 0$
1.0	0.9547	0.9547	0.9547
2.0	1.4714	1.4714	1.4714
3.0	1.8961	1.8961	1.8961

Conclusions

The article is made to offer a numerical results on Casson fluid-flow towards both flat and cylindrical geometries. The key outcomes of the presents study are assembled as follow:

- The CFV shows decline curves via both β and γ.
- The CFV shows an inciting values for increasing values of both λ and K.
- The CFT shows increasing traits for the positive values of both the K and the R_d.
- The CFT distribution is found to be decreasing functionwards Pr, Q_{-}, and δ_1 but an inverse trend is seen for the Q_{+}.
- The cylindrical surface admits enlarged variations towards an involved physical parameters as compared to flat surface.

References

[1] Batra, R. L., Bigyani J., Flow of a Casson Fluid in a Slightly Curved Tube, *International Journal of Engineering Science*, *29* (1991), 10, pp. 1245-1258
[2] Sharp, M. K., Shear-Augmented Dispersion in Non-Newtonian Fluids, *Annals of Biomedical Engineering*, *21* (1993), 4, pp. 407-415
[3] Dash, R. K., *et al.*, Casson Fluid-Flow in a Pipe Filled with a Homogeneous Porous Medium, *International Journal of Engineering Science*, *34* (1996), 10, pp. 1145-1156
[4] Kameswaran, P. K., *et al.*, Dual Solutions of Casson Fluid-Flow over a Stretching or Shrinking Sheet, *Sadhana*, *39* (2014), 06, pp. 1573-1583
[5] Khalid, A., *et al.*, Unsteady MHD Free Convection Flow of Casson Fluid Past over an Oscillating Vertical Plate Embedded in a Porous Medium, *Engineering Science and Technology*, *18* (2015), 3, pp. 309-317
[6] Animasaun, I. L., Effects of Thermophoresis, Variable Viscosity and Thermal Conductivity on Free Convective Heat and Mass Transfer of Non-Darcian MHD Dissipative Casson Fluid-Flow with Suction and nth Order of Chemical Reaction, *Journal of the Nigerian Mathematical Society*, *34* (2015), 1, pp. 11-31

[7] Raju, C. S. K, Sandeep, N., Unsteady Casson Nanofluid-Flow over a Rotating Cone in a Rotating Frame Filled with Ferrous Nanoparticles: A Numerical study, *Journal of Magnetism and Magnetic Materials*, *421* (2017), Jan., pp. 216-224
[8] Nawaz, M., *et al*., Magnetohydrodynamic Axisymmetric Flow of Casson Fluid with Variable Thermal Conductivity and Free Stream, *Alexandria Engineering Journal*, *57* (2018), 3, pp. 2043-2050
[9] Rehman, K. U., *et al*., Numerical Communication for MHD Thermally Stratified Dual Convection Flow of Casson Fluid Yields by Stretching Cylinder, *Chinese Journal of Physics*, *55* (2017), 4, pp. 1605-1614
[10] Rehman, K. U., *et al*., Numerical Analysis of MHD Casson Navier's Slip Nanofluid-Flow Yield by Rigid Rotating Disk, *Results in Physics*, *8* (2018), 3, pp. 744-751
[11] Chakrabarti, A., Gupta, A. S., Hydromagnetic-Flow and Heat Transfer over a Stretching Sheet, *Quarterly of Applied Mathematics*, *37* (1979), 1, pp. 73-78
[12] Akbar, *et al*., Numerical Analysis of Magnetic Field Effects on Eyring-Powell Fluid-Flow Towards a Stretching Sheet, *Journal of Magnetism and Magnetic Materials*, *382* (2015), May, pp. 355-358
[13] Ishak, A., *et al*., Hydromagnetic-Flow and Heat Transfer Adjacent to a Stretching Vertical Sheet, *Heat and Mass Transfer*, *44* (2008), 8, 921
[14] Zeeshan, A., *et al*., Effect of Magnetic Dipole on Viscous Ferro-Fluid Past a Stretching Surface with Thermal Radiation, *Journal of Molecular Liquids*, *215* (2016), Mar., pp. 549-554
[15] Ellahi, R., *et al*., Numerical Study of Magnetohydrodynamics Generalized Couette Flow of Eyring-Powell Fluid with Heat Transfer and Slip Condition, *International Journal of Numerical Methods for Heat & Fluid-Flow*, *26* (2016), 5, pp. 1433-1445
[16] Zeeshan, A., *et al*., Mixed Convection Flow and Heat Transfer in Ferromagnetic Fluid over a Stretching Sheet With Partial Slip Effects, *Thermal Science*, *22* (2018), 6, pp. 2515-2526
[17] Bhatti, M. M., *et al*., Simultaneous Effects of Coagulation and Variable Magnetic Field on Peristaltically Induced Motion of Jeffrey Nanofluid Containing Gyrotactic Microorganism, *Microvascular Research*, *110* (2017), Mar., pp. 32-42
[18] Ellahi, R., *et al*., On Boundary-Layer Nanoferroliquid-Flow under the Influence of Low Oscillating Stretchable Rotating Disk, *Journal of Molecular Liquids*, *229* (2017), Mar., pp. 339-345
[19] Bhatti, M. M., *et al*., Heat and Mass Transfer of Two-Phase Flow with Electric Double Layer Effects Induced Due to Peristaltic Propulsion in the Presence of Transverse Magnetic Field, J*ournal of Molecular Liquids*, *230* (2017), Mar., pp. 237-246
[20] Hassan, M., *et al*., Particle Shape Effects on Ferrofuids Flow and Heat Transfer under Influence of Low Oscillating Magnetic Field, *Journal of Magnetism and Magnetic Materials*, *443* (2017), Dec., pp. 36-44
[21] Rehman, K. U., Malik, M. Y., Application of Shooting Method on MHD Thermally Stratified Mixed Convection Flow of Non-Newtonian Fluid over an Inclined Stretching Cylinder, *Journal of Physics: Conference Series*, *822* (2017), 1, 012012
[22] Khan, A. A., *et al*., Mass Transport on Chemicalized Fourth-Grade Fluid Propagating Peristaltically through a Curved Channel with Magnetic Effects, *Journal of Molecular Liquids*, *258* (2018), May, pp. 186-195
[23] Bhatti, M. M., *et al*., Mathematical Modelling of Heat and Mass Transfer Effects on MHD Peristaltic Propulsion of Two-Phase Flow through a Darcy-Brinkman-Forchheimer Porous Medium, *Advanced Powder Technology*, *29* (2018), 4, pp. 1189-1197
[24] Hayat, T., *et al*., Magnetohydrodynamic Flow of Powell-Eyring Fluid by a Stretching Cylinder with Newtonian Heating, *Thermal Science*, *22* (2018), 01, pp. 371-382
[25] Azimi, M, Rouzbeh R., The MHD Go-Water Nanofluid-Flow and Heat Transfer between Two Parallel Moving Disks, *Thermal Science*, *22* (2016), 1, pp. 383-390
[26] Rahman, M. M, Salahuddin, K. M., Study of Hydromagnetic Heat and Mass Transfer Flow over an Inclined Heated Surface with Variable Viscosity and Electric Conductivity, *Communications in Non-Linear Science and Numerical Simulation*, *15* (2010), 8, pp. 2073-2085
[27] Ellahi, R., *et al*., A Study of Heat Transfer in Power Law Nanofluid, *Thermal Science*, *20* (2016), 6, pp. 2015-2026
[28] Milani, S., *et al*., Numerical Study of Surface Radiation and Combined Natural-Convection Heat Transfer in a Solar Cavity Receiver, *International Journal of Numerical Methods for Heat and Fluid-Flow*, *27* (2017), 10, pp. 2385-2399
[29] Rehman, K. U., *et al*., Dual Stratified Mixed Convection Flow of Eyring-Powell Fluid over an Inclined Stretching Cylinder with Heat Generation/Absorption Effect, *AIP Advances*, *6* (2016), 7, 075112

[30] Rehman, K. U., *et al*., Magneto-Nanofluid Numerical Modelling of Chemically Reactive Eyring-Powell Fluid-Flow Towards Both Flat and Cylindrical an Inclined Surfaces: A Comparative Study, *AIP Advances*, *7* (2017), 6, 065103
[31] Awais, M., *et al.*, A Computational Analysis Subject to Thermophysical Aspects of Sisko Fluid-Flow over a Cylindrical Surface, *The European Physical Journal Plus*, *132* (2017), 9, 392
[32] Bidin, B., Roslinda, N., Numerical Solution of the Boundary-Layer Flow over an Exponentially Stretching Sheet with Thermal Radiation, *European Journal of Scientific Research*, *33* (2009), 4, pp. 710-717
[33] Mukhopadhyay, S., The MHD Boundary-Layer Flow and Heat Transfer over an Exponentially Stretching Sheet Embedded in a Thermally Stratified Medium, *Alexandria Engineering Journal*, *52* (2013), 3, pp. 259-265

Paper submitted: April 24, 2018
Paper revised: May 20, 2018
Paper accepted: June 5, 2018